PERGAMON

Radiation Physics and Chemistry 53 (1998) 1–18

Radiation Physics and Chemistry

Electron inelastic-scattering cross sections in liquid water

Michael Dingfelder *, Detlev Hantke, Mitio Inokuti [1], Herwig G. Paretzke

GSF, National Research Center for Environment and Health, Institute of Radiation Protection, Ingolstädter Landstraße 1, 85764 Neuherberg, Germany

Received 15 August 1997; accepted 6 November 1997

Abstract

Electron inelastic-scattering cross-section data for use as input in electron track-structure calculations in liquid water are re-examined and improved. The dielectric-response function used in such cross-sections is estimated on the basis of optical data and other experimental and theoretical information. The mean excitation energy for stopping power is obtained to be 81.8 eV, which is close to the recent experimental value, 79.75 ± 0.5 eV, of Bichsel and Hiraoka. Inelastic-scattering cross sections are evaluated within the first Born approximation. Electron-exchange effects and semi-empirical corrections to account for non-Born effects at low energies are also incorporated.

1. Introduction

Charged particle track-structure analysis (Paretzke, 1987) is a useful basis for the understanding of early physical and chemical stages of radiation actions on matter in general. This holds true especially in radiation biology, i.e. in research on the effects of radiation on the biological cell, which has a highly inhomogeneous spatial and chemical structure. Track-structure analysis based on computer simulations requires as input data cross sections for the interactions of electrons and other charged particles with molecules in matter under consideration. In the biological cell of soft tissues, water is the dominant component (ICRU, 1989, 1992) and is largely in the liquid state. However, because of the scarcity of experimental and theoretical knowledge on detail of the molecular, chemical consequences of energy transferred in inelastic collisions, earlier track structure calculations for radiation biophysics have been using water in the vapour state as a model substance (Paretzke, 1974, 1987, 1988). Later on, cross sections for water clusters were also derived (Long et al., 1989; Long and Paretzke, 1991) to study the influence of phase effects in water in detail.

Cross sections for electron and other charged-particle collisions with molecules have been studied for many decades. An indication of the current status of the knowledge may be obtained from a recent survey (Inokuti, 1996), an IAEA-report (IAEA, 1995) and a monograph (Inokuti, 1994). As seen in the above references, recent progress in this area is substantial. With this recognition in mind, we have reviewed cross-section data for liquid water now used in track-structure studies and attempted to improve them in the light of newer information and ideas, both experimental and theoretical.

2. Scope

The present paper deals with electron inelastic-collisions with water. Electron energies considered were in the range from MeV's down to electronic excitation levels of a few eV. Throughout we shall discuss the physics underlying our treatment. We will document our procedure for determining cross sections in full

* Corresponding author. Fax: +49-89-3187-3363; E-mail: dingfelder@gsf.de.

[1] Permanent address: Argonne National Laboratory, Physics Division, Argonne, IL 60439, U.S.A.

0969-806X/98/$19.00
PII: S0969-806X(97)00317-4

detail so that others may reproduce our numerical data for their own use.

3. Method

3.1. The first Born approximation

Basically we follow the general idea of Ritchie and co-workers (Ritchie et al., 1991). For the determination of the cross sections for electrons and other charged particles *at high speeds*, it is most efficient to use the framework of the Bethe theory (Bethe, 1930, 1933; Fano, 1963; Inokuti, 1971; Landau and Lifshitz, 1970; see also addenda in Inokuti et al., 1978), based on the first Born approximation (FBA). Here we mean by 'high speeds' any speed much higher than that of an atomic or molecular electron that becomes excited or ionised (which is about the Bohr speed $e^2/\hbar = c/137 \cong 2.19 \times 10^8$ cm s^{-1} in the valence shell and thus corresponds to the electron kinetic energy of one Rydberg, 1Ry $= me^4/2\hbar^2 = 13.6$ eV).

For considerations of the interaction of charged particles with liquid water or any other condensed matter, it is appropriate to use the dielectric-response function, as fully discussed by Landau and Lifshitz (1970) and also by Fano (1963). Provided that an external charged particle is sufficiently fast, the dielectric response of matter upon sudden transfer of energy E and momentum $\hbar K$ is given in terms of the function $\epsilon(E, K)$, a characteristic of matter, which is defined as follows. Suppose that an applied electric field $\vec{E}$ dependent on time and space induces in matter an electric displacement $\vec{D}$, which is necessarily dependent on time and space and that the electric field is sufficiently weak. Then, one may write $\vec{D} = \hat{\epsilon}\vec{E}$, where $\hat{\epsilon}$ is an integral operator involving time and space variables. When both $\vec{E}$ and $\vec{D}$ are decomposed into Fourier components at frequency $E/\hbar$ and wave number K, the operator is represented by a multiplicative complex coefficient $\epsilon(E, K)$. In general, $\vec{D}$ and $\vec{E}$ are not necessarily parallel and $\epsilon(E, K)$ is a tensor. However, in what follows, we treat a scalar function $\epsilon(E, K)$ representing the average over the spatial orientation. According to the FBA, the probability of energy transfer E and momentum transfer $\hbar K$ is proportional to $\mathrm{Im}[-1/\epsilon(E, K)]$.

It is often convenient to use the system of atomic units, in which the length is expressed in units of the Bohr radius $a_0 = \hbar^2/me^2$, the momentum in units of $\hbar/a_0 = me^2/\hbar$ and the energy in units of Hartrees; 1 Hartree $= me^4/\hbar^2 = 2$Ry.

3.2. The dipole limit

A basic task is to determine $\epsilon(E, K)$ numerically at all values of E and K. One begins with $K = 0$, viz. the dipole limit, which applies to soft collisions in which the external particle glances the target molecule at a large impact parameter. An electron energy-loss spectrum for forward scattering (Inokuti, 1971; Schattschneider, 1986) gives the E-dependence of the probabilities of such collisions. One also obtains relevant data from measurements of optical properties of the material under consideration (Palik, 1985).

Following the general theory best explained by Landau and Lifshitz (1970), one first adopts a plausible dependence of $\epsilon_2(E, 0) = \mathrm{Im}\epsilon(E, 0) \geq 0$ for $E > 0$. The non-negative property reflects the fact that the material absorbs energy. When a value of $\epsilon_2(E, 0)$ for $E \leq 0$ is required in certain calculations, one extends the function using the relationship $\epsilon_2(E, 0) = -\epsilon_2(-E, 0)$.

Perhaps to facilitate numerical work, Ritchie et al. (1991) used a linear superposition $\epsilon^{(D)}$ of the Drude functions to approximate ϵ. In the original Drude model, one considers an electron subject to a harmonic binding force $-m\omega_j^2 x$ plus a damping force $-mg_j\dot{x}$, where x is the displacement, ω_j is the characteristic angular frequency and $g_j > 0$ is the damping coefficient. The electron is also subject to a force $-e\exp(-\mathrm{i}\omega t)$ due to a spatially uniform electric field of unit strength. Then, the electron gives rise to a dipole moment $(e^2/m(\omega_j^2 - \omega^2 - \mathrm{i}g_j\omega)^{-1}\exp(-\mathrm{i}\omega t)$. If there are n electrons per unit volume, the induced polarisation is $(4\pi ne^2/m)(\omega_j^2 - \omega^2 - \mathrm{i}g_j\omega)^{-1}$ and the dielectric response function $\epsilon^{(D)}(E, 0)$ is

$$\epsilon^{(D)}(E, 0) = 1 + \frac{\omega_\mathrm{p}^2}{\omega_j^2 - \omega^2 - \mathrm{i}g_j\omega}, \tag{1}$$

where $\omega_\mathrm{p}^2 = 4\pi ne^2/m$ is the plasma angular frequency.

For convenience, one may recast the above expression in the form

$$\epsilon^{(D)}(E, 0) = 1 + \frac{E_\mathrm{p}^2}{E_j^2 - E^2 - \mathrm{i}\gamma_j E}, \tag{2}$$

using the photon energy $E = \hbar\omega$ as the variable, the characteristic oscillator energy $E_j = \hbar\omega_j$, the oscillator energy width $\gamma_j = \hbar g_j$ and the plasmon energy of free electrons

$$E_\mathrm{p} = \hbar\omega_\mathrm{p} = \hbar(4\pi ne^2/m)^{1/2} = 4\sqrt{\pi}(na_0^3)^{1/2}\mathrm{Ry}. \tag{3}$$

We may rewrite Eq. (3) in a form easier for numerical evaluation. Suppose that the material consists of N molecules per unit volume and that each molecule has mass A measured in atomic mass units and contains Z electrons. Then, $n = NZ$ and a nominal (because molecular orbit electrons are not free) plasmon energy E_p can be calculated

$$E_\mathrm{p} = 28.816\left(\frac{\rho Z}{A}\right)^{1/2}\ \mathrm{eV}, \tag{4}$$

where ρ is the density of the material in g/cm^3. For water, $A = 18.0153$, $Z = 10$ and $\rho = 0.9982$ at 20°C under 1 atm. Accordingly, $E_p = 1.578$Ry $= 21.46$ eV for liquid water. Notice that the plasmon energy used here is only nominal; it merely dictates the right behaviour of $\epsilon^{(D)}(E, 0)$ at $E \gg E_j$, viz. the approach to the response of an essentially free electron (like in a gas plasma).

Eq. (2) implies the following expressions for the real and imaginary parts:

$$\epsilon_1^{(D)}(E, 0) \equiv \mathrm{Re}\,\epsilon^{(D)}(E, 0) = 1 + \frac{E_p^2(E_j^2 - E^2)}{(E^2 - E_j^2)^2 + \gamma_j^2 E^2}, \tag{5}$$

and

$$\epsilon_2^{(D)}(E, 0) \equiv \mathrm{Im}\,\epsilon^{(D)}(E, 0) = \frac{E_p^2 \gamma_j E}{(E^2 - E_j^2)^2 + \gamma_j^2 E^2}. \tag{6}$$

The dielectric response of any real material cannot be fully described by the Drude model, which presumes the binding by a harmonic force, thus permits no ionisation and fails to account for greatly different binding energies depending on the electron shell structure. Indeed, in a comprehensive analysis of $\epsilon(E, 0)$ of metallic aluminium (Shiles et al., 1980; Smith et al., 1985) and its applications (Inokuti and Smith, 1982), it was found that the Drude model fits realistic data in limited domains of E, with parameters E_j and γ_j specific to each of the domains. In other words, no single choice of E_j and γ_j enables one to fit the data over the entire range of E.

One way to treat data over the entire range of E is to use a linear superposition of the Drude functions with different values of E_j and γ_j, viz. to set (Ritchie et al., 1991)

$$\epsilon_2(E, 0) = E_p^2 \sum_j f_j \frac{\gamma_j E}{(E^2 - E_j^2)^2 + \gamma_j^2 E^2}, \tag{7}$$

where f_j is the effective number of oscillators characterised by E_j and γ_j and treat f_j, E_j and γ_j as fitting parameters. One must choose f_j so that the sum rule

$$\int_0^\infty E\epsilon_2(E, 0)\,\mathrm{d}E = \frac{\pi}{2} E_p^2 \tag{8}$$

is satisfied; this ensures the correct behaviour of $\epsilon_2(E, 0)$ at high E (Landau and Lifshitz, 1970). Then, the Kramers–Kronig relationship (Landau and Lifshitz, 1970)

$$\epsilon_1(E, 0) = 1 + \frac{1}{\pi} P \int_{-\infty}^{+\infty} \frac{\epsilon_2(E', 0)}{E' - E}\,\mathrm{d}E', \tag{9}$$

where P stands for the Cauchy principal value, enables one to obtain

$$\epsilon_1(E, 0) = 1 + E_p^2 \sum_j \frac{f_j(E_j^2 - E^2)}{(E_j^2 - E^2)^2 + \gamma_j^2 E^2}. \tag{10}$$

In the present work we follow the approach by Ritchie et al. (1978, 1991) and Hamm et al. (1975), but introduce some improvements. The linear superposition of the Drude functions leads to a non-vanishing value of $\epsilon_2(E, 0)$ for $E < E_j$, i.e. the energy absorption probability is finite at all values of $E > 0$. This result is inconsistent with the real property of water, or even of any ordinary material. In the linear-superposition model, all but a few lowest values of E_j are associated in practice with the thresholds for inner-shell excitation; then, non-vanishing values of $\epsilon_2(E, 0)$ at $E < E_j$ are particularly noticeable and are clearly unrealistic.

After deliberations on various ways for modeling $\epsilon_2(E, 0)$ best, at present we adopt the following. First, for continuum excitations (ionisations; labeled with j) we use a linear superposition of Drude forms

$$D(E, E_j) = \frac{f_j \gamma_j E}{(E_j^2 - E^2)^2 + \gamma_j^2 E^2}, \tag{11}$$

multiplied by the step function

$$\Theta(E - E_j) = \begin{cases} 0 & \text{for } E < E_j \\ 1 & \text{for } E \geq E_j \end{cases}, \tag{12}$$

and smeared out by a Gaussian function

$$G(E, E_j) = \exp\left(-\frac{(E - E_j)^2}{2\Delta_j^2}\right) \tag{13}$$

with a width Δ_j and a normalisation to $G(E = E_j, E_j) = 1$. The step function ensures no contribution at energies below the threshold. The Gaussian function represents in effect the width of the valence band including the broadening of electronic spectra due to coupling with phonons. The value of the band width has been chosen to be around $\Delta_j \approx 1$ eV (in practice between 0.6 and 1.3 eV) taking into account information about the band structure of cubic ice (Shibaguchi et al., 1977; Kobayashi, 1983; Zaider et al., 1994).

Second, for discrete excitations (labeled with k) we use the derivative Drude form (Ritchie et al., 1978, 1991)

$$D^*(E, E_k) = \frac{2 f_k \gamma_k^3 E^3}{[(E_k^2 - E^2)^2 + \gamma_k^2 E^2]^2}, \tag{14}$$

which is sharply peaked around $E \approx E_k$, and thus is more nearly discrete than the Drude form. The parameters E_k, γ_k, f_k, E_j, γ_j, f_j and Δ_j are obtained in a fit to experimental data (Heller et al., 1974). This procedure is further described in Section 4.1, and the values are displayed in Table 1 and 2.

Table 1
Parameters E_k, γ_k and f_k used for the discrete excitation part of the dielectric-response function in Eq. (15) compared to the energies E_k^{Kut} used by Kutcher and Green (1976)

		Excitations			
k	excited states	E_k (eV)	γ_k (eV)	$Z{\cdot}f_k$	E_k^{Kut} (eV)
1	$\tilde{A}^1B_1$	8.17	1.62	0.118	8.40
2	$\tilde{B}^1A_1$	10.13	2.20	0.230	10.10
3	Ryd A + B	11.31	2.10	0.1675	11.26
4	Ryd C + D	12.91	3.10	0.285	11.93
5	diffuse bands	14.50	3.90	0.280	14.10

Consequently, our model is expressed as

$$\epsilon_2(E,\,0) = E_{\mathrm{p}}^{\,2}\left\{\sum_{\mathrm{exc}\ k} D^{*}(E,\,E_k) + \sum_{\mathrm{ion}\ j}\int_{E_j-\Delta_j}^{E_j+\Delta_j} \times D(E,\,\Omega)\Theta(\Omega - E\,)G(\Omega,\,E_j\,)\,\mathrm{d}\Omega\right\}. \tag{15}$$

The Kramers–Kronig relationship, Eq. (9), allows us to evaluate $\epsilon_1(E,\,0)$. The result can be expressed analytically except for the Ω integration over the Gauss function. Appendix A gives integrals necessary for the evaluation of $\epsilon_1(E,\,0)$, as well as of the sum rule, Eq. (8).

Finally, the probability of energy transfer E from a fast charged particle at the dipole limit is given (Landau and Lifshitz, 1970; Fano, 1963) by

$$\eta_2(E,\,0) = \mathrm{Im}\,\eta(E,\,0), \tag{16}$$

where we define

$$\eta(E,\,0) = \frac{-1}{\epsilon(E,\,0)}. \tag{17}$$

In other words, the probability

$$\eta_2(E,\,0) = \frac{\epsilon_2(E,\,0)}{\epsilon_1^2(E,\,0) + \epsilon_2^2(E,\,0)} \tag{18}$$

is readily calculable. This quantity differs from $\epsilon_2(E,\,0)$, which describes energy absorption from photons, in having the denominator given in Eq. (18). The difference is insignificant for a low-density material, e.g. a dilute gas, for which $\epsilon_1(E,\,0)$ is close to unity and $\epsilon_2(E,\,0)$ is much smaller than unity over the entire spectral range. The difference between $\epsilon_2(E,\,0)$ and $\eta_2\,(E,\,0)$ is notable when $\epsilon_1(E,\,0)$ is comparable to, or even smaller than, $\epsilon_2(E,\,0)$. This occurs often in the valence-excitation domain of condensed matter. The difference is most conspicuous when $\epsilon_1(E,\,0) = 0$; indeed, this occurs in a metal for which $\epsilon_1(E,\,0) < 0$ at low E corresponding to intra-band transitions. Because $\epsilon_1(E,\,0)$ must generally approach unity at very high E, there is an energy at which $\epsilon_1(E,\,0)$ vanishes. Around there $\eta_2\,(E,\,0) = 1/\epsilon_2(E,\,0)$ has a large value. This is the plasmon excitation in the sense of Bohm and Pines (Bohm and Pines, 1953). This case does not occur in liquid water.

3.3. Finite momentum transfer

Under a broad assumption of rotational invariance (which applies to our $\epsilon(E,\,K)$ representing the average over spatial orientation), $\epsilon(E,\,K)$ is a function of K^2 and so is

$$\eta_2(E,\,K\,) = \mathrm{Im}\left(\frac{-1}{\epsilon(E,\,K\,)}\right), \tag{19}$$

Table 2
Parameters E_j, γ_j, Δ_j and f_j used for the ionisation part of the dielectric-response function in Eq. (15)

		Ionisations							
j	shells	E_j^{ion} (eV)	E_j (eV)	γ_j (eV)	Δ_j (eV)	$Z{\cdot}f_j$	$Z{\cdot}f_j^{\mathrm{eff}}$	E_j^{exp} (eV)	
1	$1b_1$	10.79	11.95	12.50	1.16	3.40	2.25	10.45[a]	10.9[c]
2	$3a_1$	13.39	14.70	16.10	1.31	3.10	2.06	13.25[a]	13.5[c]
3	$1b_2$	16.05	16.60	19.40	0.55	2.394	1.61	16.80[a]	17.0[c]
4	$2a_1$	32.30	33.30	95.0	1.00	1.595	1.21	32.40[b]	
5	K-shell	539.00	540.00	220.0	1.00	3.11	1.79	539.70[b]	

Also displayed: ionisation energies E_j^{ion} compared with binding energies taken from calculations for [a]cubic ice (Shibaguchi et al., 1977) and [b]for water vapour (Uehara et al., 1993) as well as from photoelectron spectroscopy at [c]liquid water surfaces (Faubel and Steiner, 1994).

Table 3
Parameters for the momentum transfer dependence, Eq. (20). Momentum transfer $q = \hbar K$ in atomic units

Excitations			
k	a_k	b_k	c_k
1	3.82	0.0272	0.098
2	2.47	0.0295	0.075
3	2.47	0.0311	0.074
4	3.01	0.0111	0.765
5	2.44	0.0633	0.425

which determines the probability of collisions with energy transfer E and momentum transfer $\hbar K$ (Fano, 1963; Landau and Lifshitz, 1970).

For discrete excitations k we introduce the K-dependence by using the generalised oscillator strength $f_k(K)$ in the place of f_k in Eq. (11). In general $f_k(K)$ is a decreasing function of K^2, because collisions resulting in larger and larger momentum transfers are less and less probable when one restricts energy transfers to modest values. Following Ritchie and co-workers (Hamm et al., 1975), we use

$$f_k(K) = f_k[\exp(-a_k K^2) + b_k K^2 \exp(-c_k K^2)], \tag{20}$$

where a_k, b_k and c_k are parameters. Their values are shown in Table 3.

For continua j, we introduce the K-dependence again by using the generalised oscillator strength $f_j(K)$

$$f_j(K) = f_j \frac{Z - \sum_{\text{exc } k} f_k(K)}{Z - \sum_{\text{exc } k} f_k} \tag{21}$$

in place of f_j and by replacing E_j by $E_j + (\hbar K)^2/2m$ in the Drude form (Eq. (11)). Note that f_k refers to discrete excitations. This procedure is based on the idea of an impulse approximation, in which one views a target electron as nearly free at the moment of energy and momentum transfer and accounts for its binding through its instantaneous momentum, as discussed in section 4.4 of Inokuti (1971). This procedure leads to the Bethe ridge, viz. the peaking of $\eta_2(E, K)$ around the line $E = (\hbar K)^2/2m$, with the width determined by the electron binding. The ridge describes hard collisions in which both E and K are large. Hopefully, the superposition of the Drude forms is sufficiently flexible to represent $\eta_2(E, K)$ at moderate E and K reasonably well.

3.4. The cross section differential in energy transfer

The standard term used in physics for expressing the probability of particle collisions is the cross section σ. The mean number of collisions of a specified kind that occur during the passage of an incident particle through an infinitesimal distance $\mathrm{d}x$ in a material consisting of N target particles, e.g. nuclei, atoms or molecules depending on the context, per unit volume is given by $N\sigma\,\mathrm{d}x$. For considerations of condensed matter it is convenient to use the product $N\sigma$ as an index of the collision probability which is called the macroscopic cross section in nuclear reactor physics (Weinberg and Wigner, 1958) and often designated by the symbol Σ. Notice that $\Sigma = N\sigma$ has the dimension of $(\text{length})^{-1}$ and is sometimes referred to as the 'inverse mean free path'. In what follows, we use Σ in the above sense and refer to it as 'cross section', dropping the adjective 'macroscopic' for brevity.

Let us consider the cross section $\mathrm{d}\Sigma = (\mathrm{d}\Sigma/\mathrm{d}E)\,\mathrm{d}E$ for collisions of an incident particle resulting in energy transfer between E and $E + \mathrm{d}E$ to the material. We call $\mathrm{d}\Sigma/\mathrm{d}E$ the cross section differential in energy transfer, i.e. the topic of the present section. Further, we consider the cross section $(\mathrm{d}^2\Sigma/\mathrm{d}E\,\mathrm{d}K)\,\mathrm{d}E\,\mathrm{d}K$ for collisions of the same incident particle resulting in energy transfer between E and $E + \mathrm{d}E$ *and* in momentum transfer between $\hbar K$ and $\hbar(K + \mathrm{d}K)$. Within the FBA, it is given (Fano, 1963; Landau and Lifshitz, 1970) as

$$\frac{\mathrm{d}^2\Sigma}{\mathrm{d}E\,\mathrm{d}K} = \frac{1}{\pi a_0 T K}\eta_2(E, K) \tag{22}$$

for an incident *electron* at nonrelativistic speed v, i.e. at kinetic energy $T = mv^2/2 \ll mc^2 = 511$ keV. Hence,

$$\frac{\mathrm{d}\Sigma}{\mathrm{d}E} = \frac{1}{\pi a_0 T}\int_{K_{\min}}^{K_{\max}} \eta_2(E, K)\frac{\mathrm{d}K}{K}, \tag{23}$$

where the integration limits are

$$K_{\min} = \frac{\sqrt{2m}}{\hbar}(\sqrt{T} - \sqrt{T - E}) \tag{24}$$

and

$$K_{\max} = \frac{\sqrt{2m}}{\hbar}(\sqrt{T} + \sqrt{T - E}). \tag{25}$$

For $E \ll T$ (when the FBA is best justified),

$$K_{\min} \approx \frac{E}{\hbar v} \tag{26}$$

is small in general and approaches zero at high T. In contrast,

$$K_{\max} \approx 2\frac{\sqrt{2mT}}{\hbar} \tag{27}$$

is large and increases with T. Recognising the above and the fact that $\eta_2(E, K)$ approaches a finite limit $\eta_2(E, 0)$ as $K \to 0$, one readily sees that $\mathrm{d}\Sigma/\mathrm{d}E$ has a well characterised analytic behaviour (Bethe, 1930, 1933; Inokuti, 1971)

$$\frac{d\Sigma}{dE} = \frac{1}{\pi a_0 T}\left[A(E)\ln\left(\frac{T}{Ry}\right) + B(E) + O\left(\frac{E}{T}\right)\right], \quad (28)$$

where $A(E)$ and $B(E)$ are functions of E derivable from $\eta_2(E,K)$. In particular, the $A(E)\ln(T/Ry)$ term represents the contributions from soft collisions due to dipole interactions; indeed,

$$A(E) = \frac{1}{2}\eta_2(E, 0). \quad (29)$$

The derivation of this relationship, as well as a detailed treatment of $B(E)$, is given in Appendix B. Here we point out only a property of $B(E)$, i.e. that

$$B(E) \longrightarrow 4\pi^2 n a_0^3 \left(\frac{Ry}{E}\right)^2 \quad (30)$$

at high E (exceeding all the binding energies). This asymptotic behaviour is physically obvious: $d\Sigma/dE$ should approach the sum of the Rutherford cross sections for free electrons in the material under consideration.

An additional consideration concerns the indistinguishability of an incident electron from a target electron after a collision with large energy transfer. Thus, the high-E behaviour of $B(E)$ should reflect the Mott cross section, rather than the Rutherford cross section. Recall that the Mott cross section for a collision of an electron of (nonrelativistic) kinetic energy T with a free electron at rest is expressed as

$$\frac{d\sigma_{Mott}}{dW} = \frac{4\pi a_0^2 Ry^2}{T}\left[\frac{1}{W^2} - \frac{1}{W(T-W)} + \frac{1}{(T-W)^2}\right], \quad (31)$$

where W is the kinetic energy of the slower of the two electrons after the collision. It is customary to call this slower electron the secondary electron and the other, faster, electron the primary electron. The $1/W^2$ term in the square brackets corresponds to the Rutherford cross section, and is often called the direct term. The other two terms represent a consequence of the electron indistinguishability, often referred to as 'electron-exchange term'.

In reality, a target electron is neither free nor at rest initially, but is bound to a molecule. To account for this fact, the Mott cross section has been modified. It is usual to replace the energy of the secondary electron W with $W + I$, where I is the binding energy of the ejected electron. The energy of the primary, scattered electron remains to be T–W (ICRU, 1996).

The binding energy depends on a sub-shell, or a molecular orbital, occupied by bound electrons. Suppose that the sub-shell s is occupied by Z_s electrons with binding energy I_s. Then the electron-exchange contribution to the cross section differential in E per molecule is

$$\frac{d\sigma_{exch}}{dE} = \frac{4\pi a_0^2 Ry^2}{T}\sum_s Z_s \times\left[\frac{-1}{E(T-E+I_s)} + \frac{1}{(T-E+I_s)^2}\right]. \quad (32)$$

Consequently, the macroscopic cross section including the electron-exchange contribution is written as

$$\frac{d\Sigma}{dE} = \frac{1}{\pi a_0 T}\left[A(E)\ln\left(\frac{T}{Ry}\right) + B(E) + C(T, E)\right], \quad (33)$$

where $A(E)$ and $B(E)$ are the same as in Eq. (28), and $C(T, E)$ is defined as

$$C(T, E) = 4\pi^2 a_0^3 Ry^2 \sum_s n_s \times\left[\frac{-1}{E(T-E+I_s)} + \frac{1}{(T-E+I_s)^2}\right], \quad (34)$$

where $n_s = NZ_s$ is the number of electrons in the sub-shell s per unit volume. This result is trustworthy at T far exceeding $E - I_s$, but is not usable at T close to $E - I_s$. Clearly, the first (negative) term in the square brackets is more important than the second term; thus $C(T, E) < 0$. In the Fano plot, i.e. the plot of $T\,d\Sigma/dE$ against $\ln T$, one generally sees a gradual departure from the Bethe straight line downwards at lower T (Inokuti, 1971).

Sometimes the binding effect is accounted for more precisely by incorporating into $B(E) + C(T,E)$ additional terms of $O(I_s Ry^2/E^3)$, as discussed in section 2.5 of the ICRU (1996) Report (see equation (2.10) in particular). However, we find it expedient to treat in effect those terms together with other non-FBA effects at lower T, to be fully discussed in Section 3.7.

3.5. Other cross sections and related quantities

The cross section for all collisions leading to a specified product s is given by

$$\Sigma_s = \int p_s(E)\left(\frac{d\Sigma}{dE}\right) dE, \quad (35)$$

where $p_s(E)$ is the probability of producing s upon energy transfer E. Among many quantities of interest, the first is the total cross section for inelastic scattering

$$\Sigma_{tot} = \int\left(\frac{d\Sigma}{dE}\right) dE, \quad (36)$$

where the integral is taken over all possible values of E. The second is the cross section for the excitation of a discrete level l

$$\Sigma_l = \int p_l(E)\left(\frac{d\Sigma}{dE}\right) dE, \quad (37)$$

where $p_l(E)$ is the probability of exciting level l upon

energy transfer E. This is a sharply peaked function representing the width of the level. The third is the total cross section for ionisation

$$\Sigma_{\text{ion}} = \int p_{\text{ion}}(E)\left(\frac{\mathrm{d}\Sigma}{\mathrm{d}E}\right)\mathrm{d}E, \tag{38}$$

where $p_{\text{ion}}(E)$ is the probability of producing an ion of any kind upon energy transfer E, as discussed in detail in chapter 5 of the IAEA (1995) Report. The quantity Σ_{ion} can be further classified according to a particular ion species produced (e.g. H_2O^+, H^+ or O^+ in water).

It is also important for track-structure analysis to know the cross section for producing secondary electrons of a fixed kinetic energy W, as fully discussed by Wilson et al. (1984) (see also the ICRU (1996) Report 55). This cross section $\mathrm{d}\Sigma/\mathrm{d}W$ is given by

$$\frac{\mathrm{d}\Sigma}{\mathrm{d}W} = \int \frac{\mathrm{d}p(E,\ W)}{\mathrm{d}W}\left(\frac{\mathrm{d}\Sigma}{\mathrm{d}E}\right)\mathrm{d}E, \tag{39}$$

where $[\mathrm{d}p(E,\ W)/\mathrm{d}W]\,\mathrm{d}W$ is the probability for producing secondary electrons with kinetic energies between W and $W + \mathrm{d}W$ and includes contributions from all the electron shells.

Another quantity of importance to the Monte Carlo simulation of the track structure (Paretzke, 1987) is the probability $P(E)$ that energy transfer not exceeding E occurs upon a single collision. It is defined by

$$P(E) = \frac{1}{\Sigma_{\text{tot}}}\int_{E_1}^{E} (\mathrm{d}\Sigma/\mathrm{d}E)\,\mathrm{d}E, \tag{40}$$

where the lower limit E_1 is the lowest possible excitation energy.

Finally, the mean energy loss per unit pathlength of an incident electron is given by

$$S = \int_0^\infty E\left(\frac{\mathrm{d}\Sigma}{\mathrm{d}E}\right)\mathrm{d}E, \tag{41}$$

where the integral is taken over all possible values of E.

All the quantities discussed above depend on the incident electron energy in the same way as $\mathrm{d}\Sigma/\mathrm{d}E$, discussed in Section 3.4. In other words, $T\,\mathrm{d}\Sigma/\mathrm{d}E$ should approach a linear function of $\ln T$ at $T \gg E$, as first pointed out for cross sections by Fano (1956). Therefore, we call the plot of $T\,\mathrm{d}\Sigma/\mathrm{d}E$ against $\ln T$ the Fano plot (Inokuti, 1971). For the stopping power, the plot of TS against $\ln T$ was first used by Lindhard and Scharff (1953).

3.6. Relativistic speeds

At electron kinetic energies appreciable compared to the electron rest energy $mc^2 = 511$ keV, the Bethe cross section formula, Eq. (28), needs to be modified in two respects. First, one must use relativistic kinematics to relate momentum transfer with the scattering angle and energy transfer. Second, one must account for interactions transverse to $\vec{K}$ in addition to the Coulomb interactions (which are longitudinal to $\vec{K}$), as fully discussed by Fano (1956, 1963).

The result may be written as

$$\frac{\mathrm{d}\Sigma}{\mathrm{d}E} = \frac{1}{\pi a_0 T^*}\left[A(E)\left\{\ln\frac{\beta^2}{1-\beta^2} - \beta^2\right\} + B^*(E)\right], \tag{42}$$

where $T^* \equiv mv^2/2$ (not the kinetic energy) and $\beta = v/c$. The coefficient $A(E)$ remains the same as in Eq. (29). This result arises because Eq. (26) for $K_{\min}$ remains true in relativistic kinematics and because the transverse interactions at low K can be expressed in terms of the dipole matrix element. The new coefficient $B^*(E)$ is related to $A(E)$ and $B(E)$ as

$$B^*(E) = B(E) + A(E)\ln\left(\frac{\hbar c}{e^2}\right)^2, \tag{43}$$

where the coefficient of $A(E)$ has the value 9.8405.

The behaviour of the cross section at relativistic speeds is simplest on the Fano plot, viz. a plot of $\beta^2\,\mathrm{d}\Sigma/\mathrm{d}E$ against $\ln[\beta^2/(1-\beta^2)] - \beta^2$ and is represented by a straight line with the slope given by $A(E)$ and the (extrapolated) intercept with the horizontal axis by $B^*(E)$. When plotted as a function of the kinetic energy T, the cross section decreases with increasing T in the keV region and reaches a minimum around 1 MeV, whose precise position depends weakly on the ratio $B^*(E)/A(E)$, as seen in Fig. 2 of Rieke and Prepejchal (1972). The increase at higher energies is due to the transverse interactions (Fano, 1956) and often is called the relativistic rise. Although the behaviour of the cross section at relativistic speeds as sketched above is well established by theory and also by experiments, for example, by Rieke and Prepejchal (1972) for electrons and by Ishimaru et al. (1995) for protons, the subject matter is occasionally misunderstood. An example of misunderstanding is seen in Pimblott et al. (1990), who state "The difference (between the relativistic and non-relativistic cross sections) is about 2% at 1 MeV, 10% at 10 MeV and 28% at 100 MeV" on page 491, left column. Moreover, Fig. 1 of Pimblott et al. (1990) shows no relativistic rise of the cross section up to 100 MeV. The use of the data by Rieke and Prepejchal (1972) leads to the value $8.66 \times 10^{-2}\pi a_0^2$. In other words, the relativistic cross section is greater than the nonrelativistic cross section by a factor of 4.33. It remains obscure how Pimblott et al. arrived at their statement.

The electron-exchange effect, as discussed in Section 3.4, can be accounted for at relativistic speeds by considering the Møller cross section in place of the Mott cross section, Eq. (31). Indeed, this is important for the evaluation of the stopping power for electrons

(ICRU, 1984). However, for the evaluation of $d\Sigma/dE$ itself at moderately relativistic speeds (and at lower E, where the dipole $A(E)$ term dominates), the electron-exchange effect is generally inappreciable.

Finally, the cross-section data given in the present paper are directly usable at electron energies up to several MeV. At higher energies a correction for the density effect and an additional consideration of bremsstrahlung production are necessary. At highly relativistic speeds, the Fermi density effect (Fermi, 1940) reduces the cross section by an amount depending on the total electron density and the speed. The reduction of the stopping power of liquid water due to this effect is about 1.2% at the electron kinetic energy of 1 MeV ($\beta = 0.936$), about 11.5% at 10 MeV ($\beta = 0.99997$) and about 21.5% at 100 MeV, according to the ICRU (1984) Report 37. Further on, a relativistic electron loses energy also through bremsstrahlung, in addition to inelastic scattering with molecules. The bremsstrahlung contributes about 0.7% to the total stopping power of liquid water at electron kinetic energy of 1 MeV, about 8% at 10 MeV and a significant 52% at 100 MeV (ICRU, 1984).

3.7. Corrections at low speeds

As widely known, the FBA is less and less justifiable at lower and lower speeds of an incident electron. Indeed, a large volume of experimental data for atoms and molecules in the gas phase, seen for instance in IAEA (1995) and Inokuti (1994), indicates that cross sections based on the FBA are often an overestimate by nearly a factor of two around $T \approx 100$ eV (where the total ionisation cross section shows a maximum) and even more below. For liquid water unfortunately, we are unaware of experimental data indicating how departures from the FBA set in at low T. Likewise, no comprehensive and readily usable theory seems to have been developed for generating cross sections at T comparable to E. Consequently, we must adopt a semiempirical approach for treating such cross sections.

Let us briefly review some of the approaches seen in the literature. First, one may follow the approach by Douthat (1975, 1979), Gerhart (1975), Eggarter (1975) and Kimura and Inokuti (1987) in their calculations of the yields of ions and excited states and ions in helium, hydrogen, neon and argon gases. In these studies, cross sections at T comparable to E were determined from a survey of experimental data and were numerically handled. The numerical handling of the data in a tabular form is most advantageous for its flexibility, for instance, to incorporate details of the T- and E-dependence as deemed necessary, but is inconvenient for documentation and use in further calculations such as track-structure analysis. Second, Jain and Khare (1976), Khare and Meath (1987), Mayol and Salvat (1990), Khare et al. (1993) and others introduced in effect analytic modifications of the FBA expression, Eq. (23). This line of approach is attractive for its simplicity and clarity and has led to successes in representing some of the data, e.g. the total ionisation cross section of water vapour as seen in Fig. 3.16 of the IAEA (1995) Report. However, with respect to the cross section differential in E, this line of approach falls short of being fully reliable. See, for instance, Fig. 3.33 of the IAEA (1995) Report, which compares the spectrum of secondary electrons for helium evaluated by Khare and Meath (1987) with experimental data. Finally, Rudd (1991), Rudd et al. (1992) and Kim and Rudd (1994) developed a more flexible though phenomenological approach for representing the spectra of secondary electrons for many atoms and molecules including H_2O in gas.

After full deliberation on these semiempirical approaches and fragmentary data, we decided to adopt an approach similar to that one of Paretzke (1988) for water vapour. We introduce an empirical correction factor $\Phi_j(T)$ for every ionisation shell j and Φ_k for every excitation k with the following analytical representation

$$\Phi_{k/j}(T) = \begin{cases} 0 & \text{for } T \le E_{k/j} \\ 1 - \exp[d_{k/j}(T/E_{k/j} - 1)] & \text{for } T > E_{k/j} \end{cases}, \tag{44}$$

where E_k and E_j are the excitation energies and ionisation energies, respectively. The parameters d_k and d_j (see Table 4) are obtained by analysing various experimental data in water vapour. No correction is applied to the K-shell of oxygen. The corrected singly differential cross section then reads

$$\frac{d\Sigma'}{dE} = \sum_k \Phi_k(T)\frac{d\Sigma_k}{dE} + \sum_j \Phi_j(T)\frac{d\Sigma_j}{dE}. \tag{45}$$

Table 4
Parameters d_k and d_j used in the semi-empirical low energy correction factor for different excitation and ionisation levels

Excited states	d_k
$\tilde{A}^1B_1$	−0.25
$\tilde{B}^1A_1$	−0.25
Ryd A + B	−0.25
Ryd C + D	−0.25
Diffuse bands	−0.25
Ionisation levels	d_j
$1b_1$	−0.14
$3a_1$	−0.18
$1b_2$	−0.21
$2a_1$	−0.40

A more detailed description can be found in the paper of Paretzke (1988).

Somewhat surprisingly, the low-energy correction as described above does not seem to be used in some of the track-structure calculations. For instance, Uehara et al. (1993) as well as Ritchie et al. (1991) do not mention this topic. The use of the FBA cross section with the electron-exchange terms alone leads to a significant overestimate at T close to E. This is seen in stopping-power values summarised in Fig. 8.1 of the ICRU (1984) Report. The result by Ritchie et al. (1978), who used the FBA plus the electron-exchange terms, is considerably higher at 100–1000 eV than that one of Kutcher and Green (1976), who used a form of the low-energy correction.

4. Results

4.1. Parameters

In this section we describe our numerical procedure and the results. The first step is to calculate the dielectric-response function $\epsilon_2(E, 0)$, Eq. (15), for our model and to obtain the model-parameters. For electronic excitations we use a parametrisation similar to that of Kutcher and Green (1976), however allowing changes in the overlapping part to continuum excitations ($E > 10.8$ eV) for a better agreement there while keeping the contribution of the discrete excitations to the sum rule (Eq. (8)) constant at the value of Kutcher and Green (1976). Therefore we consider five excitation levels $\tilde{A}^1B_1$, $\tilde{B}^1A_1$, Rydberg A + B, Rydberg C + D and 'diffuse bands'. We do not use 'plasmon excitations' explicitly, because there is no convincing evidence for their existence in liquid water (LaVerne and Mozumder, 1993). Dipole forbidden transitions are implicitly included in the fitting parameters for the K dependence. We succeed in fitting $\epsilon_2(E, 0)$ to experimental data (Heller et al., 1974) together with the ionisation part and obtaining values for the parameters f_k, E_k and γ_k. The Rydberg C + D excitations and the 'diffuse bands' are shifted towards higher energies (0.4 to 1.0 eV) compared to those of Kutcher and Green (1976) and are slightly broadened. This allows us to omit the introduction of a 'collective excitation' in the cross section model to achieve satisfactory agreement with the experimental data. The values used in calculations are shown in Table 1 together with the energy values used by Kutcher and Green.

In the fitting procedure to experimental data for ionisations we include only the three outermost shells (designated by the molecular orbital symbols $1b_1$, $3a_1$ and $1b_1$), because these optical data stop at an energy of 26.5 eV and the ionisation energy of the next shell (named $2a_1$) most likely exceeds this value. As a starting point for the ionisation energies we use values known from cubic ice ($E_1 = 10.45$ eV, $E_2 = 13.25$ eV, $E_3 = 16.8$ eV, according to model calculations (Zaider et al., 1994); $E_1 = 10.5$ eV, according to experiment (Shibaguchi et al., 1977)) and from photoelectron spectroscopy at liquid water surfaces ($E_1 = 10.9$ eV, $E_2 = 13.5$ eV, $E_3 = 17.0$ eV (Faubel and Steiner, 1994)). Notice that the E_1 values are considerably lower than the first ionisation threshold 12.6 eV of water vapour, chiefly owing to the solvation effect in liquid. It is physically expected that the main contribution to the ionisation cross section should come from the outermost shell ($1b_1$); indeed, this is the case with our model. The parameters for the innermost two shells ($2a_1$ and K-shell of oxygen) are chosen similar to those for the vapour phase (Paretzke, 1988) using the relation between the differential oscillator strength distribution df/dE and the dielectric-response function $\epsilon(E, 0)$

$$\eta_2(E, 0) = \mathrm{Im}\left(\frac{-1}{\epsilon(E, 0)}\right) = \frac{\pi}{2}\frac{E_p^2}{Z}\frac{1}{E}\frac{df}{dE}. \tag{46}$$

Furthermore, the parameters are adjusted to fulfil the sum rule (Eq. (8)), which we call S_1. The contribution of the K-shell of oxygen to this oscillator sum is well known (Wheeler and Bearden, 1934; Inokuti et al., 1981); a value of 1.79 is used here.

The resulting parameters E_j, γ_j, Δ_j and f_j are shown in Table 2. The ionisation energies $E_j^{\mathrm{ion}} = E_j - \Delta_j$ agree well with calculated values for ice (Zaider et al., 1994) and vapour (Uehara et al., 1993) as well as with those obtained in experimental photoelectron spectroscopy at liquid water surfaces (Faubel and Steiner, 1994). The values of γ_j of Table 2 are comparable to, or even larger than, the corresponding E_j values. This might appear physically implausible. However, the actual width of the spectrum, $\epsilon_2(E, 0)$ or $\eta_2(E, 0)$, is not simply related to γ_j because we use the step-function cut-off as given in Eq. (12). The equation

$$\sum_{k=1}^{5} f_k + \sum_{j=1}^{5} f_j = Z \tag{47}$$

derived from the sum rule Eq. (8) holds only for full Drude functions, while Eq. (8) is valid in general. 'Effective' values f_j^{eff}, i.e. the contributions to the sum rule Eq. (8), which we have called S_1, were calculated and are also displayed in Table 2.

Finally, some qualifications are appropriate concerning our procedure. The main purpose of the present article is to provide certain improvements in some of the input data used in track-structure analysis. Our procedure described above should be reasonably adequate for the description of electron tracks, but remains schematic for a detailed description of various molecular species produced. To determine the cross

section for producing a specific product such as ions, one needs to know the probability $p_{\mathrm{ion}}(E)$, or the quantum yield, of ionisation of Eq. (38). Indeed, $p_{\mathrm{ion}}(E)$ and probabilities for other decay modes in gases have been a subject of extensive studies as seen in chapter 5 of the IAEA (1995) Report and in Hatano (1994, 1996). A part of the knowledge from these studies was used in distinguishing ionisation from excitation in the region of energy transfer E where both are possible. Studies now extended to liquids (Koizumi et al., 1992; Barnas and Grand, 1994) indicate that this topic is intimately connected to the kinetics of various initial products. Therefore, a full treatment of this topic is beyond the scope of the present article.

4.2. The dielectric-response function

After determining the parameters in the fit, we evaluate $\epsilon_2(E, 0)$ of Eq. (15) and $\epsilon_1(E, 0)$ using Eq. (9) with the integrals of Appendix A. Both results are displayed in Fig. 1 together with the experimental data (Heller et al., 1974) used in the fit. In addition to $\epsilon_2(E, 0)$ on the left side of Fig. 1, the contributions from all dipole excitations and the three lowest ionisation levels are shown. The experimental data were obtained by measuring the optical reflectance and then calculating the dielectric function using a Kramers–Kronig analysis. They have considerable uncertainties, especially for $E > 20$ eV (Heller et al., 1974). Our model agrees well with these experimental data and shows only small deviations in the energy region around 20 eV. The energy loss function $\eta_2(E, 0) = \epsilon_2(E)/(\epsilon_1^2(E) + \epsilon_2^2(E))$, however, is very sensitive in this energy region where $\epsilon_1(E) \approx \epsilon_2(E)$. Our model function is lower than the experimental data at around $E \approx 20$ eV which, however, are especially uncertain here. Fig. 2 shows $\eta_2(E, 0)$ of our model compared with the experimental data (Heller et al., 1974) and a calculation by Ritchie (1996).

A more critical test of the dielectric-response function is possible by the sum rules and the mean excitation value. As already mentioned, the imaginary part $\epsilon_2(E, 0)$ has to fulfil sum rule S_1, as defined in Eq. (8). Furthermore there is another sum rule for the energy loss function, which we call S_2

$$S_2 = \int_0^\infty E\eta_2(E, 0)\,\mathrm{d}E = \frac{\pi}{2}E_{\mathrm{p}}^2 = 723.5\ (\mathrm{eV})^2. \tag{48}$$

Third, the mean excitation energy I is defined as

$$\ln \mathrm{I} = \frac{1}{\mathrm{S}_2}\int_0^\infty \mathrm{E} \ln \mathrm{E}\eta_2(\mathrm{E}, 0)\,\mathrm{dE}. \tag{49}$$

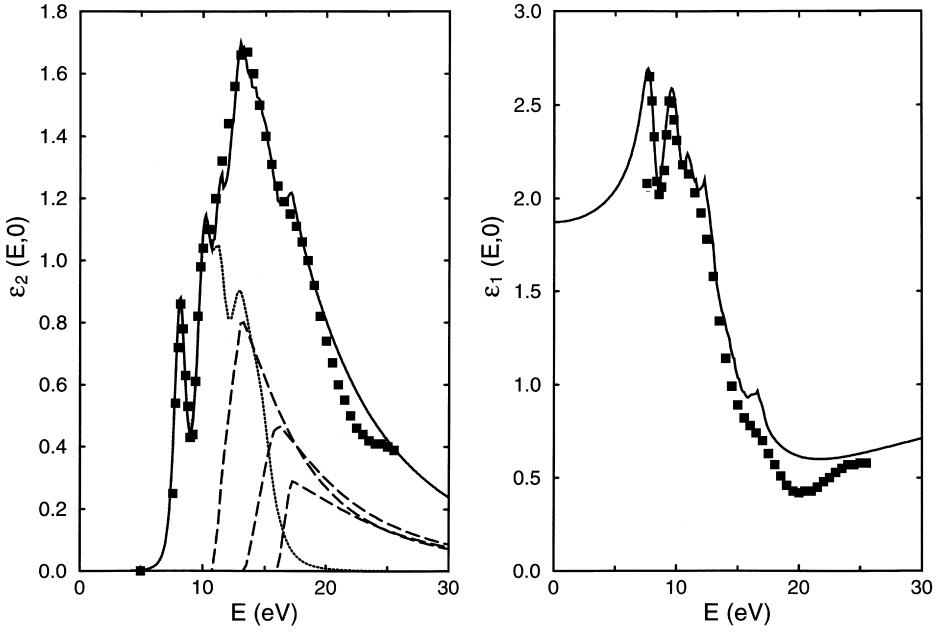

Fig. 1. Dielectric-response function $\epsilon(E, 0)$ versus energy transfer E. The left panel shows the imaginary part $\epsilon_2(E, 0)$. The solid curve represents the present result. The measurements by Heller et al. (1974) are indicated by the squares. The other curves represent contributions from excitations (dotted) and from ionisation of shells 1, 2 and 3 (dashed). The right panel shows the real part $\epsilon_1(E, 0)$ calculated from $\epsilon_2(E, 0)$ with the Kramers–Kronig relationship, again with measurements by Heller et al. (1974) as indicated by the squares.

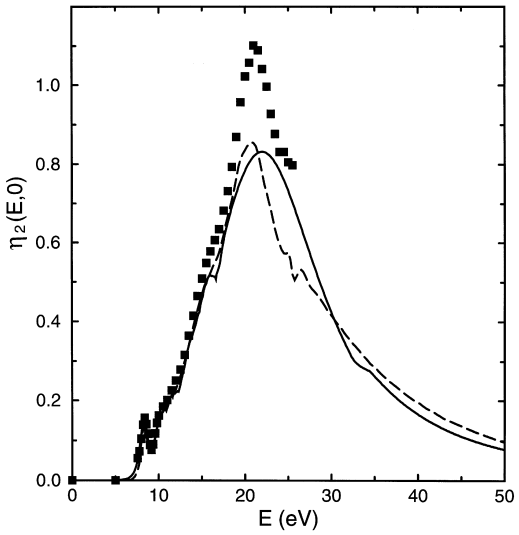

Fig. 2. Energy-loss function $\eta_2(E, 0)$ versus energy transfer E. The solid curve represents the present result, compared with measurements by Heller et al. (1974) indicated by the squares. The dashed curve represents the result obtained from Ritchie (1996).

Our parameters were adjusted to fulfil the sum rule S_1. A numerical integration of $\epsilon_2(E, 0)$ gives a value of $S_1 = 723.52$ (eV)^2, which agrees well with the theoretical value off $(\pi/2)E_p^2 = 723.5$ (eV)^2. As for the other sum rule, we obtain a similar result $S_2 = 723.50$ (eV)^2. The calculated mean excitation value I turns out to be $I = 81.8$ eV. This value is slightly higher than the earlier adopted value 75 ± 3 eV (ICRU, 1984; IAEA, 1995), but it is close to the new value 79.75 ± 0.5 eV, measured by Bichsel and Hiraoka (1992) and reported by Paul and Berger in the IAEA (1995) Report. The difference of our value from the Hiraoka–Bichsel value may come from the fact that the use of a simple Drude form to represent an ionisation shell may not be flexible enough to describe full details of the dielectric response.

4.3. Cross sections

After adding the momentum-transfer dependence to the dielectric-response function as described in Section 3.3, the values of the parameters a_k, b_k, and c_k are shown in Table 3, we can calculate the cross section differential in energy transfer in the FBA as described in Section 3.4. We recast Eq. (23) in a form appropriate for our model specifically including the shell structure. The differential FBA cross section for a single excitation k or ionisation j is then given by

$$\frac{d\Sigma^{k/j}}{dE}(E, T) = \frac{1}{\pi a_0 T} \int_{K_{\min}(E, T)}^{K_{\max}(E, T)} \frac{\epsilon_2^{k/j}(E, K)}{\epsilon_1^2(E, K) + \epsilon_2^2(E, K)} \frac{dK}{K}, \tag{50}$$

where $\epsilon_2^k(E, K)$ is the contribution of the excitation k and $\epsilon_2^j(E, K)$ the contribution of the ionisation shell j to ϵ_2. The energy transfer ranges up to $E_{\max} = T$ and the momentum transfer from $K_{\min}(E, T)$ to $K_{\max}(E, T)$ as defined in Eqs. (24) and (25).

For ionisations we further consider the threshold behaviour as well as exchange corrections to the singly differential cross section. A precise evaluation of exchange-corrected cross sections for electrons interacting with condensed matter would be quite complicated. We use a semiempirical scheme reported by Ritchie et al. (1991) for correcting for exchange effects the singly differential cross section from Eq. (23). This scheme is based on the formal analogy with the Mott cross section, Eq. (31). Thus we write

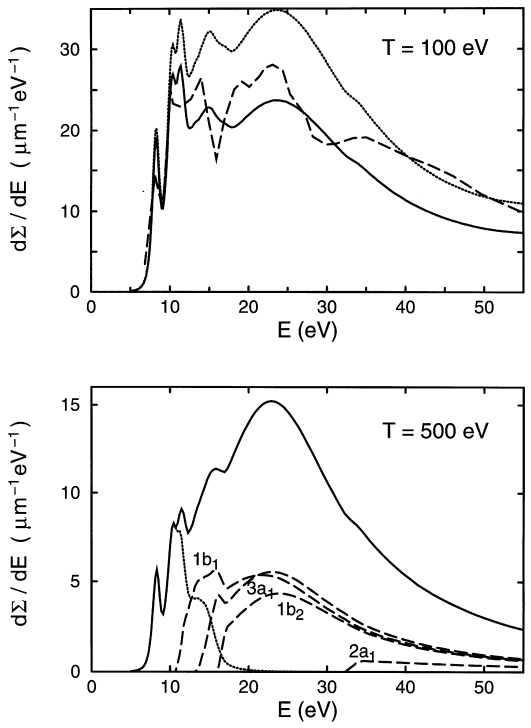

Fig. 3. Differential cross sections $d\Sigma/dE$ versus energy transfer E. The upper plot shows $d\Sigma/dE$ for an incident electron energy $T = 100$ eV (solid line) compared with the results from Hamm et al. (1975) (dashed curve). The plot also contains the calculation without low-energy correction (dotted curve). The lower plot shows $d\Sigma/dE$ (solid curve) for an incident electron energy $T = 500$ eV together with its contributions from excitations (dotted curve) and different ionisation shells (dashed curves).

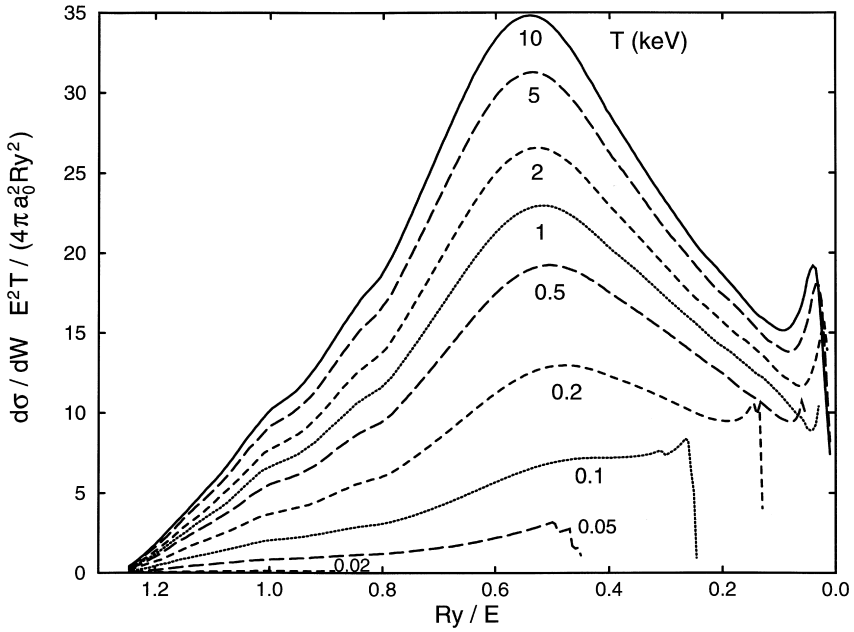

Fig. 4. Platzman plots of the differential ionisation cross section $d\sigma/dW$ per molecule for the ejection of electrons with kinetic energy W. The ordinate represents $(E^2T/4\pi a_0^2 Ry^2)(d\sigma/dW)$, where T is the incident electron energy and $E = W + B_1$, B_1 being the first ionisation threshold. The abscissa represents Ry/E. Different curves correspond to different T values.

$$\frac{d\tilde{\Sigma}^j}{dE}(E, T) = \frac{d\Sigma^j}{dE}(E, T) + \frac{d\Sigma^j}{dE}(T + E_j - E, T)$$

$$-\left(1-\sqrt{\frac{E_j}{T}}\right)\left(\frac{d\Sigma^j}{dE}(E, T)\cdot\frac{d\Sigma^j}{dE}(T+E_j-E, T)\right)^{1/2}, \quad (51)$$

where E_j is the binding energy of the shell. The energy transfer ranges from $E_{min} = E_j$ to $E_{max} = (T + E_j)/2$.

The total differential cross section then sums up to

$$\frac{d\Sigma}{dE}(E, T) = \sum_{k=1}^{5}\frac{d\Sigma^k}{dE}(E, T) + \sum_{j=1}^{5}\frac{d\tilde{\Sigma}^j}{dE}(E, T). \quad (52)$$

We add low energy corrections for incident electron energies of $T < 500$ eV as described in Section 3.7. The values of the parameters d_k and d_j are shown in Table 4. For higher incident electron energies ($T > 5$ keV) we use the relativistic Bethe approach, Eq. (42), as described in Section 3.6. Fig. 3 shows the macroscopic singly differential cross section $d\Sigma/dE$. The upper plot shows $d\Sigma/dE$ for an incident electron energy of $T = 100$ eV (solid curve) compared to the same cross section without low-energy correction (dotted curve) and compared to an earlier calculation of Hamm et al. (1975) (dashed curve). The lower plot shows $d\Sigma/dE$ for an incident electron energy of $T = 500$ eV together with its decomposition in an excitation part (dotted curve) and several ionisation levels (dashed curves; starting from left to right: $1b_1$, $3a_1$, $1b_2$ and $2a_1$).

The differential ionisation cross sections are displayed in Fig. 4 in the form of a Platzman plot (ICRU, 1996). This is a simple but very powerful way to graphically represent and analyse such data. Here the ratio Y of the microscopic cross section differential in the secondary electron energy W, $d\sigma/dW$, to the Rutherford cross section for a single electron is plotted as a function of Ry/E where $E = W + E_{j=1}^{ion}$ is the sum of the secondary electron kinetic energy W and

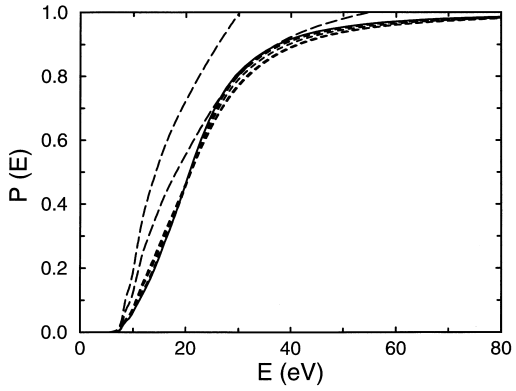

Fig. 5. The probability $P(E)$ of energy transfer not exceeding E, plotted against E for different incident electron energies T. The curves represent, starting from left to right, $T = 50$ and 100 eV (long dashed curves); 500 eV, 1, 10 and 100 keV (short dashed curves) and 1 MeV (solid curve).

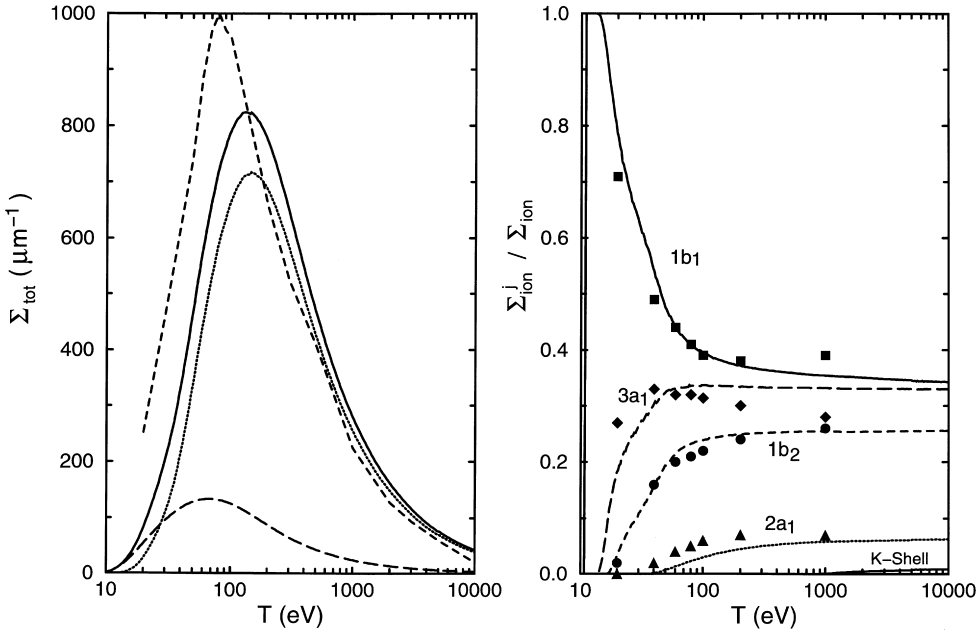

Fig. 6. Total inelastic-scattering cross section Σ_{tot} versus incident electron energy T. The left panel shows Σ_{tot} indicated by the solid curve, the contributions from excitations indicated by the long dashed curve, the contributions from ionisations indicated by the dotted curve and an earlier calculation of Ritchie et al. (1978) indicated by the short dashed curve. The right panel shows a further breakdown of the contributions Σ_{ion} from ionisation. The ordinate represents the ratio $\Sigma^j_{ion}/\Sigma_{ion}$, where j indicates each ionisation shell. The points represent data for water vapour taken from Paretzke (1988).

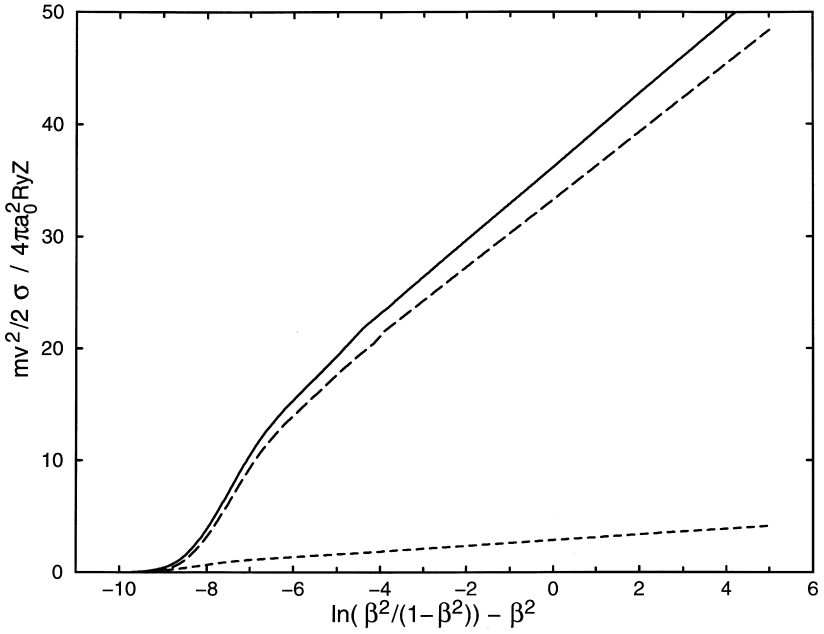

Fig. 7. Fano plots for the total cross sections for inelastic-scattering (solid curve), ionisation (long dashed curve) and excitation (short dashed curve). The ordinate represents $(mv^2/2)(\sigma/4\pi a_0^2 \mathrm{Ry}Z)$ where σ is the cross section per molecule. The abscissa represents $\ln(\beta^2/(1-\beta^2)) - \beta^2$. The slope of the asymptotic straight line for each plot is the dipole matrix element squared for the corresponding final states.

the lowest binding energy $E_{j=1}^{\text{ion}}$:

$$Y = \frac{\mathrm{d}\sigma}{\mathrm{d}W}\frac{TE^2}{4\pi a_0^2 \mathrm{Ry}^2} \tag{53}$$

Note that the area under the curve corresponds to the ionisation cross section multiplied by T, viz. the ordinate quantity in a Fano plot, apart from a universal constant factor. The shape of Y versus $1/E$ differs from one atom or molecule to another and the shape for the liquid phase of water looks different from that for the gas phase (Paretzke, 1987). Both have a maximum at around $\mathrm{Ry}/E \approx 0.55$, which corresponds to a secondary electron energy of $W \approx 14$ eV. The maximum is sharper and higher in the liquid phase, while the gas phase has an additional maximum at $\mathrm{Ry}/E \approx 0.85$ ($W \approx 5$ eV), which is completely missing in the liquid phase.

Fig. 5 shows the probability $P(E)$ that an energy transfer not exceeding E occurs upon a single collision, as defined in Eq. (40) for different incident electron energies T. $P(E)$ depends on T, weakly when T is high (which is of practical importance in track-structure computations) and more and more strongly when T is lower and lower. If the cross section $\Sigma(T,E)/\mathrm{d}E$ is a product of a function of T only and a function of E (as it is the case with the Rutherford cross section), then $P(E)$ is independent of T. The weak dependence of $P(E)$ on T at high T arises from the structure of the Bethe cross section, Eq. (28), where the content of the square brackets depends only weakly on T.

We obtain the total inelastic cross section Σ_{tot}, which is also called inverse mean free path (*imfp*), integrating the single differential cross section over the energy transfer (see Eq. (36)). We do this shell by shell and then sum them up. This is due to the fact that the maximum energy transfer is a function of the incident electron energy T as well as of the ionisation energies E_j in case of ionisations, as mentioned above. Σ_{tot} is displayed in Fig. 6 on the left hand side together with the contributions from the excitation and ionisation levels and compared to an earlier calculation of Ritchie et al. (1978). The right hand plot of Fig. 6 shows the contribution of the different ionisation shells (Σ_n^{ion}) to the ionisation part ($\Sigma_{\text{tot}}^{\text{ion}}$) of the total cross section compared to gas phase data (Paretzke, 1988). The outermost shell ($1b_1$) is the dominant one and similar to gas data. The contribution of the second outermost shell ($3a_1$) becomes comparable to $1b_1$ at higher incident energies and is higher than in the gas phase while the fourth shell ($2a_1$) contribution decreases compared to the gas phase. The third level ($1b_2$) remains more or less unchanged.

A further test of consistency for cross section data is provided by the Fano-plot, as already mentioned in Section 3.5. Here $T{\cdot}\sigma$ scaled with the Rutherford cross section $4\pi a_0^2 \mathrm{Ry} Z$ is plotted versus $\ln T$. This gives a straight line due to the asymptotics of the cross sections given by the Bethe formula (Eq. (28)). When used for relativistic energies one has to plot $T^*{\cdot}\sigma$ versus $\ln(\beta^2/(1-\beta^2)) - \beta^2$ where $T^* = mv^2/2$, $\beta^2 = v^2/c^2 = 1 - (m_0c^2/(T + m_0c^2))^2$ and T is the kinetic energy (see Eq. (42)). Such a relativistic Fano-plot is shown in Fig. 7. We see the straight lines for higher energies and the departure from it for lower energies. The slope of the straight line is also connected to the electric dipole transition matrix element M_{t}^2. We obtain a value of $M_{\text{t}}^2 = 3.25$ for liquid, which is smaller than the value $M_{\text{t}}^2 = 3.67$ in the gas phase (Paretzke, 1988), because the spectrum of the energy loss function for the liquid is generally pushed up to higher excitation energies on a whole. For the ionisation part we get similar values in the liquid and gas phase, $M_{\text{ion}}^2(\text{liquid}) = 2.93$ and $M_{\text{ion}}^2(\text{gas}) = 2.88$ (Paretzke, 1988).

As a last quantity we calculate the mass stopping power,

$$-\frac{\mathrm{d}E}{\rho\,\mathrm{d}x}(T) = N\left(\sum_{k=1}^{5} E_k \sigma_{\text{tot}}^k(T) + \sum_{j=1}^{5}\int_0^{\infty} E\frac{\mathrm{d}\sigma_j}{\mathrm{d}E}\,\mathrm{d}E\right), \tag{54}$$

which is shown in Fig. 8 (solid curve). Contributions from excitations (short dashed curve) are small compared to those from ionisations (long dashed curve). Other calculations, like Ashley's for low-energy electron stopping powers in liquid water (Ashley, 1982, 1988, 1990) (solid circles) or Paretzke's for water vapour (Paretzke, 1988) (solid diamonds) lead to a similar result.

5. Concluding remarks

The foregoing is a report of our work on electron inelastic scattering cross sections for liquid water for use, for example, in track-structure and other modeling studies in radiation physics, chemistry, and biology[2].

We intend to extend our work in several respects. First, we shall include in these considerations also other excitations than dipole-permitted transitions and the decay scheme of the molecule. Second, we shall extend our study to protons and other incoming particles and finally, we intend to treat components of the biological cell other than water (e.g. DNA).

[2] We offer our computer code, which has been written in C, that generates the present cross-section data. A copy can be transmitted in an electronically readable form, upon request to M. D., whose e-mail address is dingfelder@gsf.de

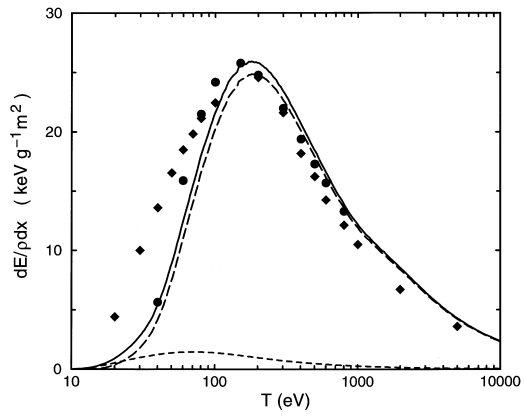

Fig. 8. Mass stopping power versus incident electron energy. The solid curve shows the result of evaluation from our cross-section data by use of Eq. (54). The short dashed curve shows the contributions from excitations and the long dashed curve the contributions from ionisations. Symbols represent results for S/ρ taken from the literature: the circle for liquid water from the IAEA (1995) Report, Table 7.6, the diamonds for water vapour from Paretzke (1987).

Acknowledgements

We thank P. Jacob for helpful discussions including valuable ideas and R. H. Ritchie for providing us with an unpublished computer code. We also thank W. Heidenreich and Y. Hatano for comments on an earlier draft. The work is supported by the European Community under Contract No. FI4P-CT95-0011 'Biophysical Models for the Induction of Cancer by Radiation' and in part by the U.S. Department of Energy under Contract No. W-31-109-Eng-38.

Appendix A. Analytical representation of the dielectric-response function

Here we present some formulas useful for the calculation of the sum rule, Eq. (8), and of $\epsilon_1(E, K)$ with the help of the Kramers–Kronig relationship, Eq. (9). We can derive these integrals doing an analytical continuation to the complex E-plane and using Riemann's residue theory. The same results can also be obtained using elementary integration methods of partial ion decomposition, integration tables and trigonometric relations. This way is simpler, but tedious. The finite $\mathrm{d}\Omega$ integration in Eq. (15) remains to be done numerically.

For the sum rule, we need the following integrals:

$$\int_0^\infty ED(E,\, E_n)\,\mathrm{d}E = \frac{\pi}{2} f_n, \tag{A.1}$$

$$\int_0^\infty ED^*(E,\, E_n)\,\mathrm{d}E = \frac{\pi}{2} f_n. \tag{A.2}$$

$$\int_0^\infty ED(E,\, E_n)\Theta(E-E_n)\,\mathrm{d}E = \begin{cases} \dfrac{\pi}{2} f_n \left\{ \dfrac{1}{2} + \dfrac{\gamma_n}{4\sqrt{4E_n^2-\gamma_n^2}} \ln\left(\dfrac{2E_n + \sqrt{4E_n^2-\gamma_n^2}}{2E_n - \sqrt{4E_n^2-\gamma_n^2}} \right) \right\}, & \text{if } 2E_n > \gamma_n; \\ \dfrac{f_n \gamma_n}{\sqrt{\gamma_n^2 - 4E_n^2}} \left\{ \dfrac{\pi}{4} \left(1 + \sqrt{1 - \dfrac{4E_n^2}{\gamma_n^2}} \right) - \dfrac{1}{2} \arctan\left(\dfrac{2E_n}{\sqrt{\gamma_n^2 - 4E_n^2}} \right) \right\}, & \text{if } 2E_n < \gamma_n. \end{cases} \tag{A.3}$$

For calculating $\epsilon_1(E,0)$ from $\epsilon_2(E,0)$ according to the Kramers–Kronig relationship, we need the following integrals. The second one can simply be obtained from the first one by differentiation with respect to parameter γ_n.

$$\frac{2}{\pi} P \int_0^\infty \frac{s}{s^2 - E^2} \frac{f_n \gamma_n s}{(E_n^2 - s^2)^2 + \gamma_n^2 s^2}\,\mathrm{d}s = \frac{f_n (E_n^2 - E^2)}{(E_n^2 - E^2)^2 + \gamma_n^2 E^2}, \tag{A.4}$$

$$\frac{2}{\pi} P \int_0^\infty \frac{s}{s^2 - E^2} \frac{2 f_n \gamma_n^3 s^3}{[(E_n^2 - s^2)^2 + \gamma_n^2 s^2]^2}\,\mathrm{d}s = \frac{f_n (E_n^2 - E^2)((E_n^2 - E^2)^2 + 3\gamma_n^2 E^2)}{[(E_n^2 - E^2)^2 + \gamma_n^2 E^2]^2}, \tag{A.5}$$

$$\frac{2}{\pi}P\int_0^\infty \frac{s}{s^2-E^2}\frac{f_n\gamma_n s}{(E_n^2-s^2)^2+\gamma_n^2 s^2}\Theta(s-E_n)\,\mathrm{d}s \tag{A.6}$$

$$= \begin{cases} \dfrac{1}{2\pi}\dfrac{f_n\gamma_n}{(E_n^2-E^2)^2+\gamma_n^2E^2}\left\{2E\ln\left|\dfrac{E_n+E}{E_n-E}\right|+\dfrac{\pi}{\gamma_n}(E_n^2-E^2)-\dfrac{E_n^2+E^2}{\sqrt{4E_n^2-\gamma_n^2}}\ln\left(\dfrac{2E_n+\sqrt{4E_n^2-\gamma_n^2}}{2E_n-\sqrt{4E_n^2-\gamma_n^2}}\right)\right\}, & \text{if } \gamma_n<2E_n; \\ \dfrac{1}{2\pi}\dfrac{f_n\gamma_n}{(E_n^2-E^2)^2+\gamma_n^2E^2}\left\{2E\ln\left|\dfrac{E_n+E}{E_n-E}\right|+\dfrac{\pi}{\gamma_n}(E_n^2-E^2)-\dfrac{2(E_n^2+E^2)}{\sqrt{\gamma_n^2-4E_n^2}}\arctan\left(\dfrac{\sqrt{\gamma_n^2-4E_n^2}}{2E_n}\right)\right\}, & \text{if } \gamma_n>2E_n \end{cases}$$

The above two expressions are analytic continuations of each other as a function of γ_n across the boundary $\gamma_n=2E_n$.

Appendix B. Coefficients $A(E)$ and $B(E)$ of Eq. (28)

Consider the integral

$$J=\int_{K_{\min}}^{K_{\max}}\eta_2(E,\,K)\frac{\mathrm{d}K}{K} \tag{B.1}$$

in Eq. (23) and its asymptotic behaviour at high T, i.e. at $T\gg E$. One may set $K_{\max}\to\infty$. The error resulting from doing so is $O(K_{\max}^{-2})=O((E/T)^{-s})$, because $\eta_2(E,K)\propto K^{-2s}$ as $K\to\infty$, s being 4 or greater (see section 3.1 of Inokuti, 1971).

Introducing a value $\bar{K}$, independent of T, that separates high-K and low-K domains, we write

$$J=\int_{\bar{K}}^{\infty}\eta_2(E,\,K)\frac{\mathrm{d}K}{K}+\int_{K_{\min}}^{\bar{K}}\eta_2(E,\,K)\frac{\mathrm{d}K}{K}. \tag{B.2}$$

We may call the first integral J_1. We rewrite the second integral as

$$\int_{K_{\min}}^{\bar{K}}\eta_2(E,\,K)\frac{\mathrm{d}K}{K}=\eta_2(E,\,0)\ln\left(\frac{\bar{K}}{K_{\min}}\right)+J_2, \tag{B.3}$$

where

$$J_2=\int_{K_{\min}}^{\bar{K}}\left[\eta_2(E,\,K)-\eta_2(E,\,0)\right]\frac{\mathrm{d}K}{K}. \tag{B.4}$$

For deriving $A(E)$ and $B(E)$, one may put $K_{\min}=0$ in Eq. (B.4). The error resulting from doing so is

$$\int_0^{K_{\min}}\left[\eta_2(E,\,K)-\eta_2(E,\,0)\right]\frac{\mathrm{d}K}{K} =\frac{1}{4}K_{\min}^2\mathrm{d}\eta_2(E,\,K)/(\mathrm{d}K^2)\big|_{K=0}=O\left(\frac{E}{T}\right). \tag{B.5}$$

Thus we write

$$J_2=\int_0^{\bar{K}}\left[\eta_2(E,\,K)-\eta_2(E,\,0)\right]\frac{\mathrm{d}K}{K}. \tag{B.6}$$

Using Eq. (24) and $T=mv^2/2$, we note that

$$\left(\frac{\bar{K}}{K_{\min}}\right)^2=\frac{\bar{K}^2\hbar^2v^2}{E^2}=4(\bar{K}a_0)^2\left(\frac{\mathrm{Ry}}{E}\right)^2\left(\frac{T}{\mathrm{Ry}}\right), \tag{B.7}$$

and may express J as

$$J=\frac{1}{2}\eta_2(E,\,0)\left\{\ln\left(\frac{T}{\mathrm{Ry}}\right)+\ln\left[4(\bar{K}a_0)^2\left(\frac{\mathrm{Ry}}{E}\right)^2\right]\right\} +J_1+J_2+O\left(\frac{E}{T}\right). \tag{B.8}$$

Comparison with Eq. (28) gives Eq. (29) and

$$B(E)=\frac{1}{2}\eta_2(E,\,0)\ln\left[4(\bar{K}a_0)^2\left(\frac{\mathrm{Ry}}{E}\right)^2\right]+J_1+J_2. \tag{B.9}$$

Note that the value of $B(E)$ is independent of $\bar{K}$, as one may readily see upon differentiation with respect to $\bar{K}$.

Although the above procedure is in essence the same as in section 4.1 of Inokuti (1971), we sketched it for establishing notations of the present paper. Their relations with equation (4.13) of Inokuti (1971) are as follows:

$$A(E)=4\pi^2Na_0^3\left(\frac{\mathrm{Ry}^2}{E}\right)\frac{\mathrm{d}f}{\mathrm{d}E} \tag{B.10}$$

and

$$B(E)=A(E)\ln(4c_{\mathrm{e}}), \tag{B.11}$$

where $\mathrm{d}f/\mathrm{d}E$ and c_{e} are the notations used by Inokuti (1971).

References

Ashley, J.C., 1982 Radiat. Res. 89, 25.
Ashley, J.C., 1988 J. Electron Spectrosc. Rel. Phen. 46, 199.
Ashley, J.C., 1990 J. Electron Spectrosc. Rel. Phen. 50, 323.
Barnas, A., Grand, D., 1994 J. Phys. Chem. 98, 3440.
Bethe, H., 1930 Ann. Phys. (Leipzig) 5, 325.
Bethe, H., 1933. In: Geiger, H., Scheel, K. (Eds.), Handbuch der Physik, Vol. 24/1. Springer, Berlin, p. 273.
Bichsel, H., Hiraoka, T., 1992 Nucl. Instrum. Methods B 66, 345.

Bohm, D., Pines, D., 1953 Phys. Rev. 92, 609.
Douthat, D.A., 1975 Radiat. Res. 64, 141.
Douthat, D.A., 1979 J. Phys. B 12, 663.
Eggarter, E., 1975 J. Chem. Phys. 62, 833.
Fano, U., 1956 Phys. Rev. 102, 385.
Fano, U., 1963 Ann. Rev. Nucl. Sci. 13, 1.
Faubel, M., Steiner, B., 1994. In: Christophorou, L.G. et al. (Eds.), Linking the Gaseous and Condensed Phases of Matter, Nato ASI Series B 326. Plenum Press, New York, p. 517.
Fermi, E., 1940 Phys. Rev. 57, 485.
Gerhart, D.E., 1975 J. Chem. Phys. 62, 821.
Hamm, R.N., Wright, H.A., Ritchie, R.H., Turner, J.E., Turner, T.P., 1975. In: Booz, J., Ebert, H. G., B.G.R. Smith (Eds.), 5th Symp. on Microdosimetry, EUR-5452. Verbania, Pallanza, Sept., p. 1037.
Hatano, Y., 1994. In: Kuchitsu, K. (Ed.), Dynamics of Excited Molecules. Elsevier, Amsterdam, p. 151.
Hatano, Y., 1996. In: Hagen, U., Harder, D., Jung, H., Streffer, C. (Eds.), Proc. 10th International Congress of Radiation Research, Würzburg, 1995. Universitätsdruckerei H. Stütz AG, Würzburg, p. 86.
Heller, J.M., Jr., Hamm, R.N., Birkhoff, R.D., Painter, L.R., 1974 J. Chem. Phys. 60, 3483.
International Atomic Energy Agency, 1995. Atomic and Molecular Data for Radiation Therapy and Related Research, IAEA-TECDOC-799. IAEA, Vienna, 1995.
International Commission on Radiation Units and Measurements, 1984. Stopping Powers for Electrons and Positrons, ICRU Report 37. International Commission on Radiation Units and Measurements, Bethesda, Maryland.
International Commission on Radiation Units and Measurements, 1989. Tissue Substitutes in Radiation Dosimetry and Measurements, ICRU Report 44. International Commission on Radiation Units and Measurements, Bethesda, Maryland.
International Commission on Radiation Units and Measurements, 1992. Photon, Electron, and Neutron Interaction Data for Body Tissues, ICRU Report 46. International Commission on Radiation Units and Measurements, Bethesda, Maryland.
International Commission on Radiation Units and Measurements, 1996. Secondary Electron Spectra from Charged Particle Interactions, ICRU Report 55. International Commission on Radiation Units and Measurements, Bethesda, Maryland.
Inokuti, M., 1971 Rev. Mod. Phys. 43, 297.
Inokuti, M., Itikawa, Y., Turner, J.E., 1978 Rev. Mod. Phys. 50, 23.
Inokuti, M., Dehmer, J.L., Baer, T., Hanson, H.D., 1981 Phys. Rev. A 23, 95.
Inokuti, M., Smith, D.Y., 1982 Phys. Rev. 25, 61.
Inokuti, M. (Ed.), 1994. Advances in Atomic, Molecular, and Optical Physics, Vol. 33: Cross-Section Data. Academic Press.
Inokuti, M., 1996. In: Hagen, U., Harder, D., Jung, H., Streffer, C. (Eds.), Proceedings of the Tenth International Congress of Radiation Research, Würzburg, 1995. Universitätsdruckerei H. Stütz AG, Würzburg, p. 49.
Ishimaru, H., Shibata, S., Inokuti, M., 1995 Phys. Rev. A 51, 4631.
Jain, D.K., Khare, S.P., 1976 J. Phys. B. 9, 1429.
Khare, S.P., Meath, W.J., 1987 J. Phys. B 20, 2101.
Khare, S.P., Saksena, V., Wadehra, J.M., 1993 Phys. Rev. A 48, 1209.
Kim, Y.-K., Rudd, M.E., 1994 Phys. Rev. A 50, 3954.
Kimura, M., Inokuti, M., 1987 J. Chem. Phys. 87, 3875.
Kobayashi, K., 1983 J. Phys. Chem. 87, 4317.
Koizumi, H., Lacmann, K., Schmidt, W.F., 1992 J. Phys. D 25, 857.
Kutcher, G.J., Green, A.E.S., 1976 Radiat. Res. 67, 408.
Landau, L.D., Lifshitz, E.M., 1970. Electrodynamics of Continuous Media (J.B. Sykes, J.S. Bell, M.J. Kearsley, Trans.) 2nd ed. Pergamon Press, London.
Lindhard, J., Scharff, M., 1953. Kgl. Danske Videnskab. Selskab. Mat.-Fys. Medd. 27, No. 15.
Long, K.A., Paretzke, H.G., Müller-Plathe, F., Diercksen, G.H.F., 1989 J. Chem. Phys. 91, 1569.
Long, K.A., Paretzke, H.G., 1991 J. Chem. Phys. 95, 1049.
Mayol, R., Salvat, F., 1990 J. Phys. B 23, 2117.
Palik, E. (Ed.), 1985 and 1989. Handbook of Optical Constants of Solids, two volumes. Academic Press, New York.
Paretzke, H.G., 1974. In: 4th Symposium on Microdosimetry, Luxembourg, EUR 5122. p. 141.
Paretzke, H.G., 1987. In: Freeman, G.R. (Ed.), Kinetics of Non-Homogeneous Processes. John Wiley and Sons, New York, p. 89.
Paretzke, H.G., 1988. Simulation von Elektronenspuren im Energiebereich 0.01–10 keV in Wasserdampf. GSF-Bericht 24/88. GSF, Neuherberg.
Pimblott, S.M., LaVerne, J.A., Mozumder, A., Green, N.J.B., 1990 J. Phys. Chem. 94, 488.
Rieke, F.F., Prepejchal, W., 1972 Phys. Rev. A 6, 1507.
Ritchie, R.H., Hamm, R.N., Turner, J.E., Wright, H.A, 1978. In: Booz, J., Ebert, H.G. (Eds.), Sixth Symposium on Microdosimetry, Brussels, Belgium, EUR-6064. Harwood Academic Publishers, London, p. 345.
Ritchie, R.H., Hamm, R.N., Turner, J.E., Wright, H.A., Bloch, W.E., 1991. In Glass, W.A., Varma, M.N. (Eds.), Physical and Chemical Mechanisms in Molecular Radiation Biology. Plenum Press, New York, p. 99.
Ritchie, R.H., 1996. Private communication.
Rudd, M.E., 1991 Phys. Rev. A 44, 1644.
Rudd, M.E., Kim, Y.-K., Madison, D.H., Gay, T.J., 1992 Rev. Mod. Phys. 54, 441.
Schattschneider, P., 1986. Fundamentals of Inelastic Electron Scattering. Springer-Verlag, Vienna.
Shibaguchi, T., Onuki, H., Onaka, R., 1977 J. Phys. Soc. Jpn. 42, 152.
Shiles, E., Sasaki, T., Inokuti, M., Smith, D.Y., 1980 Phys. Rev. B 22, 1612.
Smith, D.Y., Shiles, E., Inokuti, M., 1985. In: Palik, E. (Ed.), Handbook of Optical Constants of Solids. Academic Press, New York, p. 369.
Wilson, W.E., Miller, J.H., Toburen, L.H., Manson, S.T., 1984 J. Chem. Phys. 80, 5631.
Uehara, S., Nikjoo, H., Goodhead, D.T., 1993 Phys. Med. Biol. 38, 1841.
LaVerne, J.A., Mozumder, A., 1993 Radiat. Res. 133, 282.

Weinberg, A.M., Wigner, E.P., 1958. The Physical Theory of Neutron Chain Reactions. The University of Chicago Press, Chicago.

Wheeler, J.A., Bearden, J.A., 1934 Phys. Rev. 46, 755.

Zaider, M., Vracko, M.G., Fung, A.Y.C., Fry, J.B., 1994 Radiat. Prot. Dosim. 52, 139.